High Fill Factor and Open Circuit Voltage in Organic Photovoltaic Cells with Diindenoperylene as Donor Material

By *Julia Wagner, Mark Gruber, Alexander Hinderhofer, Andreas Wilke, Benjamin Bröker, Johannes Frisch, Patrick Amsalem, Antje Vollmer, Andreas Opitz, Norbert Koch, Frank Schreiber,* and *Wolfgang Brütting**

Small-molecule photovoltaic cells using diindenoperylene (DIP) as a new donor material in combination with the fullerene C_{60} as an electron acceptor are demonstrated. In addition to the successful application in planar and bulk heterojunction devices, a comprehensive analysis including structural studies, the determination of the energy level alignment and electrical transport investigations is given, stressing the correlation between growth conditions, film morphology, and device performance. Due to pronounced crystallinity and a large surface area of DIP films grown at elevated temperature, exceptionally high fill factors of almost 75% are achieved in planar heterojunction cells. Bulk heterojunctions exhibit large-scale phase separation forming a bicontinuous network of both molecular species, which enables efficient exciton dissociation and charge carrier transport. The high ionization potential of DIP and the favorable energy level alignment with the fullerene C_{60} yield large open circuit voltages close to 1 V and comparable power conversion efficiencies of about 4% in both cell architectures.

1. Introduction

Energy conversion utilizing organic semiconductors in photovoltaic cells has been under investigation since the 1970s.[1] After poor success with metal-organic Schottky junctions,

a seminal step towards more efficient organic photovoltaic cells (OPVC) was made by Tang in 1986,[2] who laid the foundation for effective exciton-dissociation with the invention of the donor-acceptor heterojunction concept. Since then, many different approaches for increasing the power conversion efficiency have been proposed: Amongst others, the realization of bulk heterojunctions (BHJ) from solution processed polymer-fullerene mixtures,[3,4] which reduces the exciton diffusion bottleneck by creating an interpenetrating network of donor and acceptor materials, has proven extremely successful. In recent years power conversion efficiencies under simulated sunlight conditions exceeding 7% have been achieved.[5–7] In spite of its obvious advantage to facilitate exciton dissociation and charge carrier generation, which is otherwise limited by small exciton diffusion length in organic semiconductors, the BHJ concept, however, also has some disadvantages: Blends of electronically different materials often show reduced charge carrier mobility, as compared to the neat electron and hole transporting materials,[8,9] and enhanced recombination losses, leading to reduced fill factor (FF) and open circuit voltage (V_{OC}) in solar cells.[10,11]

In the area of molecular OPVC materials, which are in the focus of this work, bulk heterojunctions have been realized with a number of different donor-acceptor combinations. Classical examples are the metal-phthalocyanines (Pc), such as CuPc or ZnPc, pentacene or oligothiophenes as donors in combination with C_{60} as acceptor or perfluorinated analogues of these donor molecules.[12–15] However, due to the afore-mentioned limitations regarding charge transport in organic semiconductor blends (see, for example, the detailed studies on CuPc:C_{60} mixtures in field-effect transistors[9] and diodes[8,16]) molecular BHJ cells usually exhibit a significantly smaller layer thickness and thus less light absorption as compared to their polymeric counterparts. Consequently, the planar heterojunction (PHJ) remains a viable alternative in the context of small molecule OPVCs, in particular, since these materials are deposited from the vapor phase which allows for preparing well-defined multilayer structures. The optimization of deposition parameters, like substrate

[*]   J. Wagner, M. Gruber, Dr. A. Opitz, Prof. W. Brütting
      Institut für Physik
      Universität Augsburg
      Universitätsstr. 1, 86135 Augsburg, Germany
      E-mail: wolfgang.bruetting@physik.uni-augsburg.de
      A. Hinderhofer, Prof. F. Schreiber
      Institut für Angewandte Physik
      Universität Tübingen
      Auf der Morgenstelle 10, 72076 Tübingen, Germany
      A. Wilke, B. Bröker, J. Frisch, P. Amsalem, Prof. N. Koch
      Institut für Physik
      Humboldt-Universität zu Berlin
      Newtonstr. 15, 12489 Berlin, Germany
      Dr. A. Vollmer
      Helmholtz-Zentrum Berlin für Materialien
      und Energie GmbH – BESSYII
      Albert-Einstein-Straße 15, 12489 Berlin, Germany

ADVANCED
FUNCTIONAL
MATERIALS
www.afm-journal.de

Materials
Views
www.MaterialsViews.com

temperature and evaporation rate, allows growing films with higher crystallinity, resulting in better transport of both charge carriers and excitons, which in turn is the prerequisite for utilizing thicker layers for improved light harvesting. Additionally, since recombination in PHJ is limited to the narrow interfacial region (or the contacts), these cells have the potential for higher fill factors in comparison to BHJ solar cells.

Besides optical absorption as well as transport and recombination properties, a decisive parameter is the open circuit voltage (V_{OC}) of a solar cell, which is given by the splitting of the quasi-Fermi levels of electrons and holes under illumination. It has been shown convincingly for polymeric solar cells that there is a direct relation between V_{OC} and the energy-level offset at the donor–acceptor heterojunction, i.e., in first order approximation the difference between the highest occupied molecular orbital (HOMO) level of the donor and the lowest unoccupied molecular orbital (LUMO) level of the acceptor or, if the exciton binding energy is considered, the energy of the intermolecular charge transfer state resulting from exciton dissociation.[17] The importance of this restrictive aspect can be demonstrated using the example of the wide-spread material system C_{60}/CuPc, on which many of the traditional small molecule solar cells are based. In spite of advantages such as efficient light harvesting due to the high absorption coefficient of CuPc over a broad spectral range, as well as the large acceptor strength of the fullerene,[18] the overall quantum efficiency is to some extend limited by the low open circuit voltage not exceeding 0.6 V.[19–22] The reason for this limitation can be found in the small intermolecular HOMO–LUMO gap of only ca. 1 eV.[23]

In this paper, we present photovoltaic cells based on the new donor material diindenoperylene (DIP) in combination with the fullerene C_{60} as acceptor. The chemical structure of DIP and the absorption spectra of DIP and C_{60} are depicted in **Figure 1**. DIP has been shown to exhibit an almost balanced transport of electrons and holes along the *c'* direction in single crystals[24] and remarkably high exciton diffusion lengths of up to 100 nm[25] –although the magnitude of the exciton diffusion length and its unique determination in thin films is still under discussion.[26–28] It was further reported that DIP exhibits

exceptionally high structural order in evaporated thin films, with molecules standing almost upright with their long axis aligned parallel to the surface normal on inert substrates.[29] This, in turn, confirms the large exciton diffusion length as there is a correlation between structural coherence length and exciton diffusion length.[30] Moreover, it was shown that these films exhibit a high hole mobility of up to 0.1 cm^2 V^{-1}s^{-1} in field–effect transistor geometry, i.e., parallel to the substrate surface.[31] To our knowledge, however, DIP has not yet been investigated in photovoltaic cells. Only recently, a similarly constructed aromatic molecule, tetraphenyldibenzoperiflanthene (DBP), was used in planar heterojunction OPVCs exhibiting an open-circuit voltage of 0.9 V and power conversion efficiencies of up to 3.6%,[32] but no correlations to film morphology, energy level alignment and transport properties are available for this material. High values for V_{OC} (close to 1 eV) were also achieved using low bandgap oligothiophenes (DCVnT) as donor material when combined with C_{60} as acceptor.[33–34] Even higher open circuit voltages reaching 1.5 V have been obtained when blending suitable electron-donating and accepting polymers, however, often showing low fill factors.[35–38]

In the following we will discuss the influence of the substrate temperature during film growth on the morphology and structural ordering of DIP films on solar cell relevant substrates. Thereafter, we will present results on the energy level alignment in photovoltaic cells with C_{60} as acceptor and demonstrate how this affects the electrical characteristics of single junctions both in the dark and under illumination before comparing the performance of planar and bulk heterojunction cells under simulated sunlight conditions.

2. Morphological and Structural Investigation

For materials with short exciton diffusion lengths the morphology is a crucial parameter as it determines on the one hand the magnitude of the photoactive volume where excitons can be efficiently dissociated. On the other hand, even in a blend with large interfacial area the successful formation of percolation paths in the donor and acceptor material is a prerequisite for efficient charge carrier collection towards the electrodes.[39] Furthermore, transport properties of both excitons and charges are strongly correlated to the crystalline order of the involved materials. We have therefore grown DIP films at different substrate temperatures and investigated their morphological and structural properties in neat films as well as in heterostructures covered with C_{60} and in blends where DIP and C_{60} were coevaporated.

Figure 2 shows the surface topography (from atomic force microscopy (AFM)) of 50 nm thick DIP films evaporated on tin-doped indium oxide (ITO)-coated glass substrates covered with a hole injection layer of poly(3,4-ethylenedioxythiophene):poly (styrenesulfonate) (PEDOT:PSS), which were heated to different temperatures during evaporation. We note that all PEDOT:PSS films heated to different temperatures showed smooth, featureless topography as probed by AFM. The surface of DIP grown on the unheated substrate (Figure 2a) indicates growth of small islands with about 80 nm in diameter. When heating the substrate to 100 °C during evaporation the surface morphology
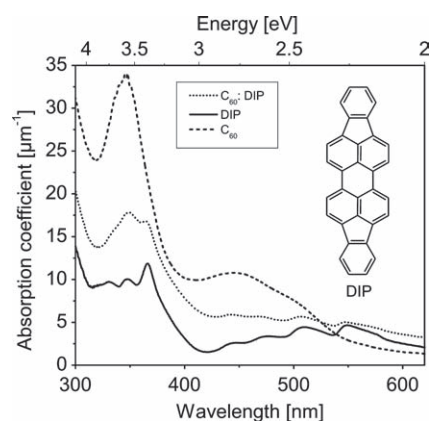

Figure 1. Absorption spectra of neat films of DIP and C_{60} and a coevaporated C_{60}:DIP film (mixing ratio 1:1 by weight). The spectra are calculated from transmission measurements on transparent substrates. The inset shows the molecular structure of DIP.
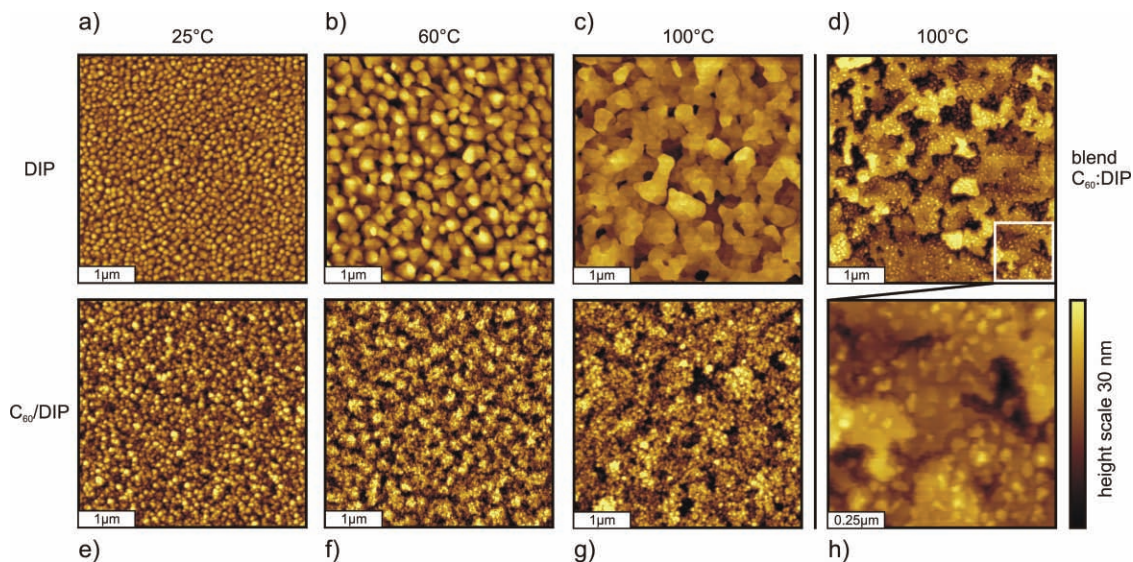
www.MaterialsViews.com

ADVANCED
FUNCTIONAL
MATERIALS
www.afm-journal.de

FULL PAPER

Figure 2. Top row: AFM images of DIP films (50 nm) on PEDOT:PSS/ITO, evaporated at substrate temperatures of a) 25 °C, b) 60 °C, and c) 100 °C. Bottom row: C_{60} (80 nm) on DIP (50nm)/PEDOT:PSS/ITO, with DIP evaporated at the same substrate temperatures as in the upper row. d) AFM image of C_{60}:DIP blend (mixing ratio 1:1, 50 nm)/DIP (5 nm) on PEDOT:PSS/ITO evaporated at substrate temperature of 100 °C with magnification in (h).

changes to a cohesive microstructure with extended crystallites (Figure 2c). More importantly, the DIP film grown at 100 °C has a large surface area which is expected to be favorable for solar cells. DIP films evaporated at an intermediate substrate temperature of 60 °C show a surface morphology that appears in between those evaporated on the unheated and the 100 °C substrate (Figure 2b). Evaporating C_{60} on top of these DIP films yields small C_{60} domains with diameters of about 25–30 nm which are adapting to the underlying morphology of the DIP film (Figure 2e–g). Coevaporation of both materials (with the substrate at 100 °C) leads to a spongiform basic structure (Figure 2d) composed of large interconnected features resembling the neat DIP film grown at 100 °C as well as smaller crystallites on top (see enlarged Figure 2h) reminiscent of C_{60} grown on top of DIP. This observation already points to phase separation in the coevaporated film which will be confirmed in the following. An additional indication for phase separation in the coevaporated film is given by the absorption spectrum of the mixed film (Figure 1), which resembles an additive superposition of the individual spectra even though roughness and reflection have not been taken into account.

In order to detect crystalline order and quantitatively determine the spatial coherence length of the observed structures, X-ray diffraction (XRD) measurements were performed. In specular diffraction the momentum transfer q is parallel to the surface normal (i.e., $q = (0,0,q_z)$, see sketch in **Figure 3**), thus probing the electron density profile along that direction. Bragg peaks are analyzed by means of the peak centre position q_z and the full width at half maximum of the peak, Δq_z. The corresponding lattice spacing is determined as $d = 2\pi/q_z$, whereas a lower limit for the vertical domain size is given by $D \approx 2\pi/\Delta q_z$.[40] Figure 3 shows X-ray reflectivity data of neat DIP films (40 nm), bilayered structures of C_{60} (20 nm) atop of DIP (20 nm) and mixed films of DIP and C_{60} (40 nm, mixing ratio 1:1 by weight), all evaporated on PEDOT:PSS/ITO substrates.

The DIP films and the mixed C_{60}:DIP layers were deposited at substrate temperatures of 25 °C and 100 °C, respectively. For all samples, Bragg reflections at $q_z = 0.378$ Å^{-1} associated with a DIP lattice plane spacing of $d_{DIP} = 16.6$ Å are observed. From this it is deduced that crystalline domains with DIP molecules standing almost upright are formed on PEDOT:PSS/ITO (tilt angle $\Phi \approx 17°$,[41] denoted as σ-phase[29,40]) as schematically sketched in Figure 3. The upright standing arrangement of the DIP molecules is consistent with the low absorption coefficient of neat DIP films (see Figure 1), as the transition dipole moment of the fundamental molecular absorption is aligned along the long molecular axis and thus unfavorably oriented for efficient absorption of light under normal incidence. DIP Bragg reflections from films evaporated at 100 °C are more intense
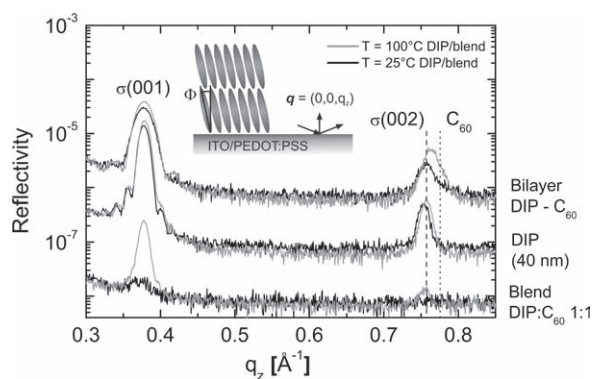

Figure 3. Specular X-ray reflectivity of DIP(40 nm) on PEDOT:PSS/ITO, C_{60}(20 nm)/DIP(20 nm) on PEDOT:PSS/ITO and mixed layers of C_{60}:DIP(40 nm, mixing ratio 1:1) on PEDOT:PSS/ITO, grown at different temperatures as indicated in the diagram. The inset shows the scattering geometry for the specular scans and a sketch of the σ–phase of DIP molecules, stacked with their long axis essentially perpendicular to the substrate (tilt-angle $\Phi \approx 17°$ with respect to the surface normal).

ADVANCED
FUNCTIONAL
MATERIALS
www.afm-journal.de

Materials
Views
www.MaterialsViews.com

FULL PAPER

compared with films grown at room temperature, which is a clear evidence for higher crystallinity.

In contrast to previous studies on neat C_{60} films evaporated on PEDOT:PSS/ITO[16] the XRD spectra of C_{60} evaporated on DIP (grown at substrate temperatures of 25 °C and 100 °C) show comparatively pronounced Bragg reflections of C_{60} at $q_z \approx 0.775$ Å^{-1} superimposed with the DIP(002) reflection. This exceptional behavior may be attributed to improved growth properties of C_{60} on top of the well ordered DIP structure. Laue oscillations around the DIP(001) Bragg reflections of the neat DIP film and the C_{60}/DIP bilayer structure are clear evidence for coherently ordered domains, whose magnitude correspond to the whole DIP layer thickness in both cases. Mixed DIP:C_{60} layers show the same DIP Bragg peak positions as neat DIP, which confirms the appearance of phase separation in coevaporated films. However, there is no measurable C_{60} Bragg reflection in the blends, which indicates low out-of-plane order for C_{60} crystallites. Nevertheless, the comparably narrow width Δq_z of the DIP(001) Bragg peak in the mixture corresponds to a coherence length of $D \approx 45$ nm, which is approximately equal to the entire layer thickness, indicating that crystalline DIP domains extend throughout the whole film. This is in full agreement with AFM measurements (cf., Figure 2) depicting the blend of DIP and C_{60} as cohesive structures of DIP with small C_{60} crystallites in between. Further details including grazing incidence X-ray diffraction data are given in section A of the Supporting Information.

3. Electronic Structure

DIP and C_{60} thickness dependent UPS (ultraviolet photoelectron spectroscopy) investigations of sample structures as they are used in OPVCs were performed in order to assess the energy level alignment in these devices. Two different commercially available PEDOT:PSS containing formulations were used: Clevios™ P AI4083 (designated as PEDOT:PSS) and Clevios™ HIL1.3 (designated as HIL1.3) providing two hole injection layers (HIL) with different work functions (see below). Specifically, the material sequences (i) C_{60}/DIP/PEDOT:PSS, (ii) C_{60}/DIP/HIL1.3 and (iii) C_{60}:DIP(codeposited)/PEDOT:PSS were chosen. While (i) and (iii) allow to compare energy levels in PHJ and BHJ structure, (ii) allows the determination of the positive pinning level of DIP and the electronic structure at the interface to the hole extracting electrode in the pinning regime,[42] because HIL1.3 has a higher work function as compared to the standard PEDOT:PSS (see also section B of the Supporting Information).

Figure 4a and b show thickness dependent UPS spectra (only one monolayer and one multilayer spectrum are shown for clarity) of the planar heterojunction (PHJ) interface of C_{60}/DIP formed on PEDOT:PSS, with an initial conducting polymer work function of 4.9 eV (secondary electron cut-off (SECO) spectra in Figure 4a). The deposition of DIP on PEDOT:PSS does not change the sample work function, i.e., no interfacial dipole is formed, indicating that energy level pinning of DIP does not yet occur at this electrode work function. No sample work function change is observed at the C_{60}/DIP interface as well, i.e., vacuum level alignment at this donor/acceptor interface is
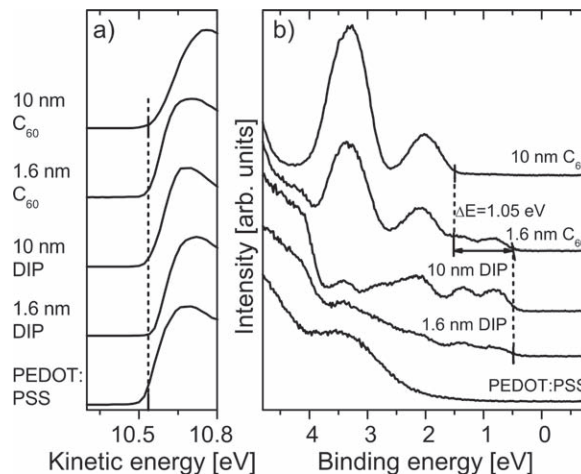
Figure 4. Ultraviolet photoelectron spectra of PEDOT:PSS/ITO substrates with different coverage of DIP and C_{60} on top of 10 nm DIP. Secondary electron cutoff (SECO) spectrum a) and valence region spectrum b).

valid. From the valence region spectra (Figure 4b) we infer that the low binding energy (BE) onset of the DIP HOMO directly at the interface (1.6 nm coverage) to PEDOT:PSS and for the multilayer (10 nm coverage) is at the same distance from the Fermi-Energy E_F, with a value of 0.45 eV. This value corresponds to the hole injection barrier at the electrode-donor interface and, adding the sample work function of 4.9 eV, yields a DIP ionization energy of 5.35 eV. The valence spectra for C_{60} on 10 nm DIP/PEDOT:PSS show that the low BE onset of the acceptor HOMO is at 1.50 eV, both for the C_{60} mono- and multi-layer. Consequently, the HOMO offset between the donor DIP and the acceptor C_{60} at this interface is 1.05 eV.

The energy level alignment at the C_{60}/DIP interface is unchanged when using the high work function HIL1.3 as electrode, i.e., vacuum level alignment prevails and the HOMO offset is 1.05 eV (see section B of the Supporting Information). However, the interface energetics between HIL1.3 and DIP are markedly different from DIP/PEDOT:PSS. Upon DIP deposition the sample work function changes from 5.70 eV (pristine HIL1.3) to 4.9 eV (see Supporting Information). This observation is consistent with pinning of the DIP energy levels due to the high initial work function of HIL1.3. Because the work function of multilayer DIP on both PEDOT:PSS and HIL1.3 is identical (4.9 eV), we can conclude that this is the critical substrate work function for energy level pinning of DIP.[42] We note that the work function of both HILs, in particular PEDOT:PSS, depends critically on the residual water content in the conductive polymer film; with decreasing water content, e.g., induced by film annealing in vacuum, the work function increases up to 5.6 eV.[43] Therefore, it is reasonable to argue that DIP/PEDOT:PSS contacts in devices fabricated at elevated substrate temperatures exhibit lower contact resistance. The energy level structure at C_{60}/DIP/HIL interfaces is schematically summarized in **Figure 5**a, where the dashed and shaded energy levels only occur when HIL1.3 is used. The C_{60}/DIP interface energetics relevant for PHJ devices are identical for both PEDOT:PSS formulations. Assuming a transport gap for C_{60} of 2.3 eV[44] and for DIP of 2.5 eV,[45] the offset between
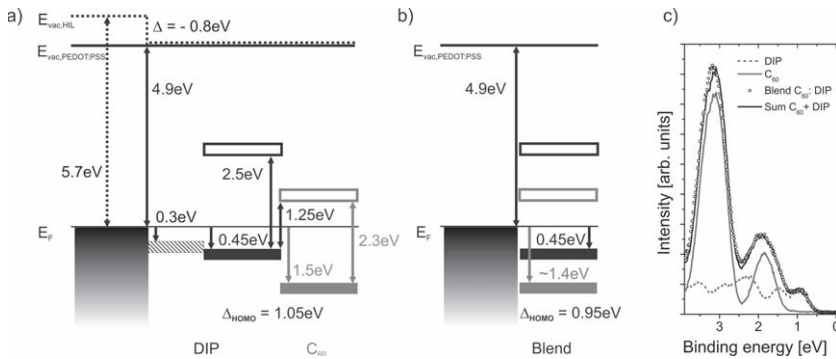
www.MaterialsViews.com

**ADVANCED
FUNCTIONAL
MATERIALS**
www.afm-journal.de

FULL PAPER

Figure 5. Schematic energy level diagrams for a) the PHJ C_{60}/DIP/HIL with PEDOT:PSS or HIL1.3 as hole injection layer and b) the corresponding BHJ. Dashed lines and the shaded area mark the levels measured for the HIL1.3. c) Valence region spectra for C_{60}, DIP and the mixed film C_{60}:DIP compared to a summation of the pristine C_{60} and DIP spectra.

the DIP HOMO and the C_{60} LUMO is 1.25 eV, which is an estimate of the maximum achievable open circuit voltage in OPVCs.[46]

In Figure 5b we show the energy level alignment for bulk heterojunction C_{60}:DIP, obtained by co-deposition of donor and acceptor material (1:1 ratio) on PEDOT:PSS. The energy levels are almost identical to the PHJ case, only the low BE onset of the HOMO level of C_{60} is found 0.1 eV closer to E_F, as inferred from a fitting routine of the mixed film UPS spectra by summation of pristine C_{60} and DIP spectra (Figure 5c). Consequently, the HOMO offset for the BHJ is 0.95 eV, and the offset between the DIP HOMO and the C_{60} LUMO is 1.35 eV. Thus, compared to the intermolecular HOMO-LUMO gap of the planar configuration (1.25 eV) similar values for V_{OC} are expected in PHJ and BHJ solar cells.

4. Electrical Characterization–Dependence on Growth Conditions

To demonstrate the importance of film growth conditions, we investigated the current-voltage (j–V) characteristics of nominally planar heterojunctions between DIP (grown at different substrate temperature) and C_{60} evaporated on top (with the underlying DIP film then kept at room temperature). This allows for a direct comparison between film morphology and the resulting electrical properties in a solar cell architecture. The structure of the investigated PHJ cells is Al(100 nm)/LiF (lithium fluoride, 0.5 nm)/C_{60}(80 nm). DIP(50 nm)/PEDOT:PSS/ITO, with DIP evaporated at substrate temperatures of 25 °C, 60 °C, and 100 °C.

Figure 6 shows the j–V characteristics for the cells in dark (dashed lines) and under one sun simulated AM1.5G solar illumination (solid lines). In the following discussion we focus on the shape of the j–V characteristics in the forward bias regime. A detailed analysis with regard to photovoltaic properties of planar and bulk heterojunction solar cells will be the subject of section 5. All different substrate temperatures yield short circuit current densities (j_{SC}) in the range between −0.8 and −1.2 mA cm^{-2} and V_{OC} between 0.85 V and 0.92 V. The j–V characteristics of the device where DIP was grown at room

temperature are strongly affected by an S-shape behavior, i.e. they show a decrease of the current close to the open-circuit voltage, which reduces the fill factor in a solar cell, and also very low current above V_{OC}. This feature decreases continuously when heating the substrate to higher temperatures during DIP deposition and vanishes completely for the device with DIP grown at 100 °C.

The occurrence of the undesired S-shape in the current-voltage characteristics under illumination is correlated to suppressed forward currents being apparent already in the dark j–V characteristics, as displayed in Figure 6b on a semi-logarithmic scale.

The forward-bias characteristics can be fitted (solid lines) using the modified Shockley equation:[47]

$$j = j_s \left\{ \exp\left[\frac{e(V - jR_s)}{nkT} \right] - 1 \right\} \tag{1}$$

where j_S is the reverse-bias saturation current density, n the ideality factor, e the electron charge, R_S a series resistance, k Boltzmann's constant, and T the temperature. The slope of the j–V characteristics in the exponential regime depends on j_S and the ideality factor n. In our devices we find an ideality factor of about 1.5 for the planar heterojunction diode with DIP evaporated at a substrate temperature of 100 °C. For the other substrate temperatures the determination of n is difficult due to the presence of the leakage currents. The most noticeable difference in the dark j–V characteristics, however, is the continuous decrease of the series resistance R_S when the substrate temperature during DIP evaporation is raised. Thus, R_S decreases by almost three orders of magnitude from 42 kΩ at room temperature to 55 Ω at 100 °C substrate temperature, causing the systematic decline of the S-shape in the j–V curves until complete vanishing at 100 °C.

S-shaped solar cell characteristics have recently gained more and more attention in the literature and are commonly ascribed to energetic injection and extraction barriers between the photoactive layer system and the electrodes.[48–50] In the present case, the S-shaped characteristics are clearly connected to the growth temperature of the DIP layer. Together with the arguments given in the previous section for a reduction of the hole injection barrier on heated PEDOT:PSS and DIP layer thickness variations (not shown here) it indicates the decisive role of charge carrier injection and transport in DIP, which are both drastically improved when the substrate is heated to 100 °C.

5. Application of DIP in Solar Cells

The applicability of DIP as donor material has already been demonstrated in the previous section, although the focus was more on the transport behavior of DIP films evaporated at different substrate temperatures. For a detailed analysis of photovoltaic properties the device stack using DIP and C_{60} as photoactive materials was extended by an additional exciton blocking material bathocuproine (BCP). The beneficial effect of BCP on solar cell performance has been demonstrated by
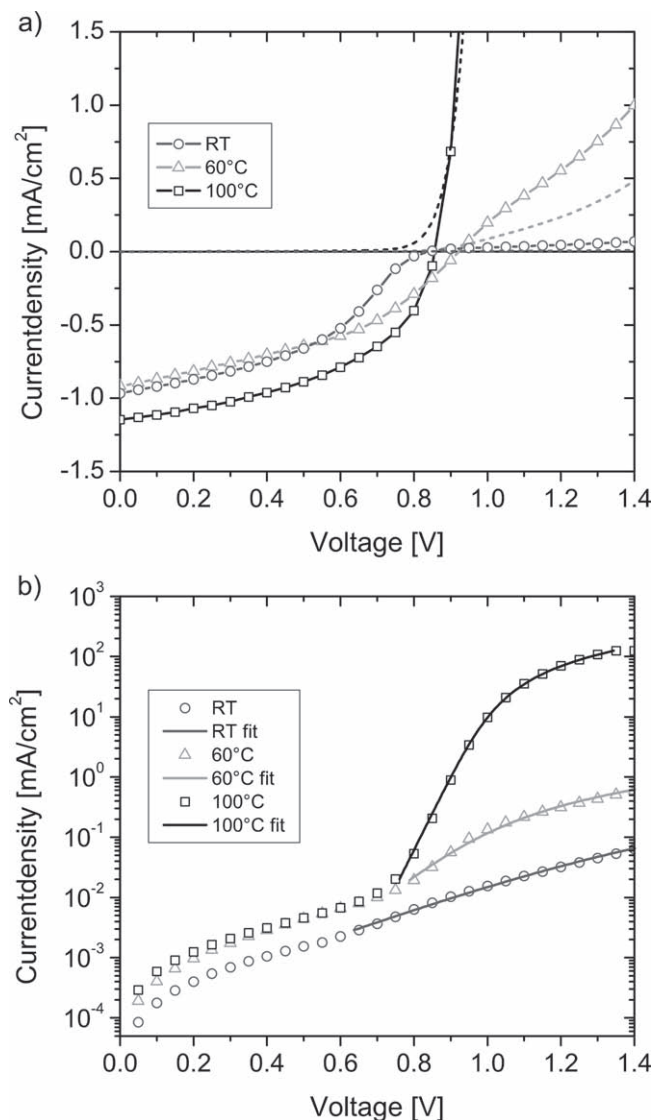
ADVANCED
FUNCTIONAL
MATERIALS
www.afm-journal.de

www.MaterialsViews.com

FULL PAPER

Figure 6. Current density vs. voltage (j–V) characteristics of PHJ diodes. The device structures are Al(100 nm)/LiF(0.3 nm)/C$_{60}$(80 nm)/DIP(50 nm)/PEDOT:PSS/ITO. During DIP evaporation the substrates were heated to different temperatures (RT, 60 °C, 100 °C). a) j–V characteristics in the dark (dashed lines) and under simulated AM 1.5G illumination at 100 mW cm^{-2}. b) Logarithmic plot of the dark j–V characteristics (open symbols). The solid lines are fits to the j–V characteristics based on the modified diode equation.

various studies, all describing its property to prohibit quenching of excitons at the electrode and to act as diffusion barrier for Al and as protection layer to eliminate the creation of Al-induced defect states in C$_{60}$.[51–53]

Planar as well as planar-mixed heterojunction (PM-HJ) devices with different thicknesses of the organic layers have been fabricated and compared to each other. The PM-HJ is a combination of a strict planar heterojunction and a mixed layer bulk heterojunction within the same structure and is known to unify the benefits of both concepts.[54] Thus, it takes maximum advantage of the unhindered charge carrier collection properties of neat organic layers, and the improved exciton

dissociation properties of films consisting of a mixture of donor and acceptor materials. The exact layer sequences of the investigated PHJ solar cells (device **A** and **C**) and the PM-HJ cells (device **B** and **D**) are given in **Figure 7**a. According to the above discussed electrical properties of C$_{60}$/DIP heterojunctions dependent on different substrate temperatures, the investigation of photovoltaic properties is restricted to cells where DIP and mixed C$_{60}$:DIP films were deposited on substrates heated to 100 °C.

The obtained current density-voltage (j–V) characteristics under one sun simulated AM1.5 illumination are shown in Figure 7b and the corresponding photovoltaic parameters are summarized in **Table 1**. In general, all four devices show almost identical open-circuit voltage V_{OC} slightly above 0.9 V and differ only in their short-circuit currents j_{SC} and fill factors (FF).

The short-circuit currents are considerably higher in the PM-HJ solar cells (devices **B** and **D**) as compared to the corresponding PHJ structures (devices **A** and **C**). Excitons which are created in the mixed layer are always in proximity of a donor-acceptor interface and can thus easily be dissociated. Furthermore, excitons created in the adjacent layer of neat DIP may also contribute to the photocurrent, as the layer thicknesses of 5 and 15 nm are well below the exciton diffusion length.[25]

Successful realization of the bulk heterojunction concept requires the formation of percolation pathways inside the mixed film, which is necessary for efficient charge carrier transport. From the morphological and structural analysis of mixed C$_{60}$:DIP films (see section 2) it can be deduced that both materials exhibit phase separation in the blend and form percolation paths for both carrier types. However, the decrease in j_{SC} from device **B** to **D** demonstrates the limits of the bulk heterojunction concept: with the increase in layer thickness, recombination losses due to the presence of both phases in close proximity exceed the gain in absorption efficiency and finally reduce j_{SC}.[55,56]

Comparing the PHJ devices **A** and **C**, j_{SC} is markedly increased from device **A** to device **C** due to the larger film thicknesses of DIP and C$_{60}$ in device **C**, leading to improved absorption of incoming light and exciton generation. The essential requirement for this enhancement is the high crystallinity and the concomitant large exciton diffusion length of DIP, facilitating efficient charge carrier dissociation and collection, respectively, even for enlarged film thickness.

The second parameter, in which the investigated cells differ in a characteristic way, is the fill factor. Both PHJ cells have a higher FF than the PM-HJ devices, at least at high light intensities (further details are given in section C of the Supporting Information) and in particular for the thick PHJ device **C** it reaches exceptionally high values exceeding 74% at one sun. This is – to the best of our knowledge – one of the highest fill factors observed for organic small molecule solar cells. It indicates highly efficient charge carrier transport towards the electrical contacts with little recombination losses[56] – despite of comparatively thick layers – as well as unhindered charge carrier extraction without energetic barriers.[12,48]

The fill factors of both PM-HJ cells are significantly below the values of device **C**, peaking at light intensities of about 10 mW cm^{-2} (device **B**: 58%, device **D**: 55%). Inherently higher bulk recombination and lower carrier mobility in the mixed
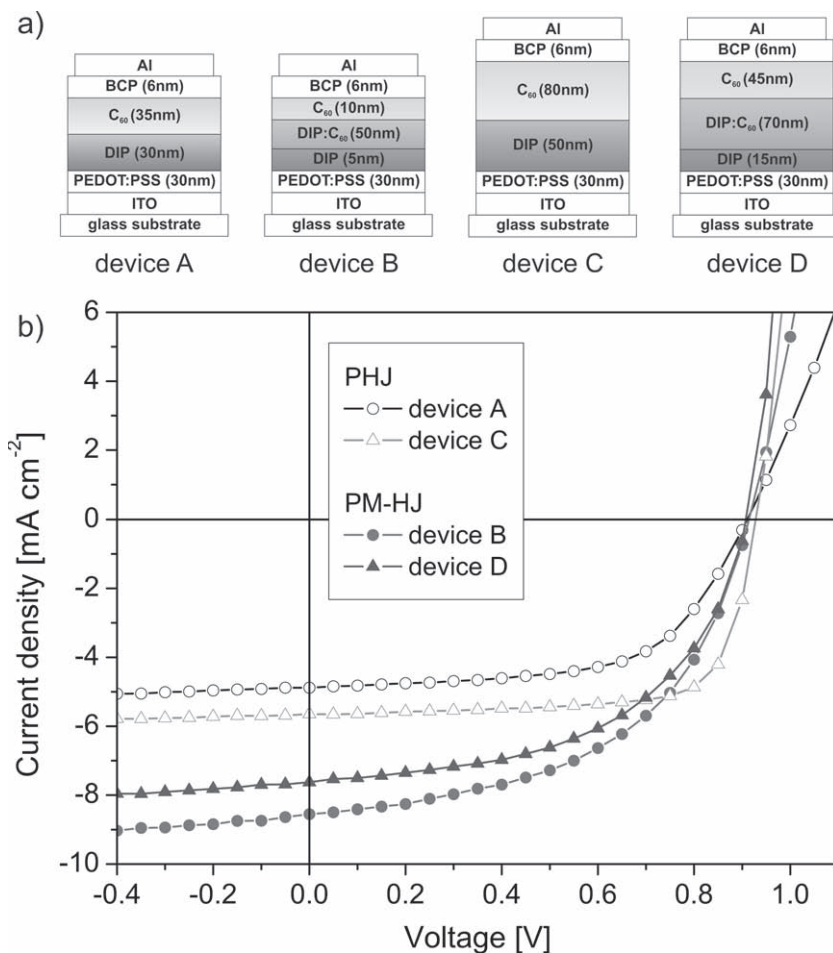
a)

b)

Figure 7. a) PHJ solar cell architecture of samples **A** and **C**, and PM-HJ architecture of samples **B** and **D**. b) Current density vs. voltage (*j*–*V*) characteristics of devices with different architecture (see a) measured under AM 1.5G illumination. During DIP evaporation (as neat or blended film) the substrates were heated to 100 °C.

layer probably limit charge collection efficiency and thereby the FF of these devices.[10,11]

As already mentioned, all devices reach open circuit voltages in excess of 0.9 V at one sun simulated AM1.5 illumination (see also section C of the Supporting Information). Thereby the V_{OC} of device **C** is slightly higher than for the other three devices. It is remarkable that the PM-HJ devices **B** and **D** reach almost the same values as the best PHJ device, while pure bulk heterojunction devices (not shown here) have lower V_{OC} (0.6–0.7 V). This can be seen as a further advantage of the hybrid PM-HJ concept over the BHJ device: in the latter V_{OC} may be limited by the built-in voltage V_{BI}, because recombination of charge carriers at the interface between an electrode and the mixed layer immediately sets in as soon as the applied voltage exceeds V_{BI}.[48] The neat donor and acceptor layers encompassing the mixed layer in the PM-HJ cell suppress this direct recombination and thus enable V_{OC} to reach values as high as for PHJ devices.

The comparison of different device architectures shows that a power conversion efficiency around $\eta_{PCE} \approx 4\%$ can be reached with a hybrid planar-mixed heterojunction structure with BCP as exciton blocking layer. Nevertheless, the hybrid

PM-HJ cell suffers from transport losses in the mixed layer, which limit the FF to values not exceeding 53% at one sun. As compared to this PM-HJ structure, the lower current in the planar heterojunction cells is almost completely compensated by their extremely high FF achieving equally high power conversion efficiency.

Finally, we would like to discuss the performance of the investigated cells in comparison to C_{60}/CuPc, which is a widely used prototype small molecule OPVC system.[20,45,57–59] For that purpose we have put together solar cell parameters obtained by us on C_{60}/CuPc devices fabricated and measured under comparable conditions (see **Table 1**, lines 5 and 6).

The most prominent difference is the open-circuit voltage being only about 0.5 V for C_{60}/CuPc cells. Theoretically the maximum value of V_{OC} is related to the difference between the HOMO energy of the donor and the LUMO level of the acceptor, minus the binding energy of the dissociated, geminate electron-hole pair.[46] Comparing the energy level alignment for C_{60}/DIP cells as discussed in section 3 and as reported by us in Ref.[23] for C_{60}/CuPc one comes to the conclusion that both from the point of view of the HOMO-LUMO gap at the donor/acceptor interface as well as the built-in voltage, resulting from the differences in the effective electrode work functions, C_{60}/DIP cells are expected to have an open-circuit voltage that is approximately larger by 0.5 V – fully consistent with the experimentally observed numbers.

Regarding the short-circuit currents both types of C_{60}/CuPc cells are clearly ahead of the corresponding DIP based devices, however, this is simply related to the larger absorption coefficient of CuPc (peak value 20.6 μm^{-1}[45]) and the better spectral coverage in the long wavelength range (bands in the range 550–780 nm.[45]) Given the fact that the maximum absorption coefficient of DIP in the visible

Table 1. Solar cell parameters of devices with different architecture as obtained from the *j*–*V* characteristics shown in Figure 7. V_{OC}: open circuit voltage, j_{SC}: short circuit current density, FF: fill factor, η_{PCE}: power conversion efficiency. For comparison, characteristic values for C_{60}/CuPc cells taken from Ref.[45] are given.

Device	Architecture	V_{OC} [V]	j_{SC} [mA cm^{-2}]	FF [%]	η_{PCE} [%]	Reference
A	PHJ	0.91	−4.8	60.4	2.7	This work
B	PM-HJ	0.91	−8.4	51.9	4.1	This work
C	PHJ	0.93	−5.7	74.3	3.9	This work
D	PM-HJ	0.91	−7.5	53.1	3.7	This work
CuPc/C_{60}	PHJ	0.54	−7.3	52.6	2.3	[45]
CuPc/C_{60}	PM-HJ	0.49	−10.6	33.4	1.8	[45]

spectral range (420–580 nm) is about four times lower than for CuPc, the reduction of the photocurrent (by only about 25%) for DIP cells is remarkably small and points towards very good carrier collection.

The lower fill factors for C_{60}/CuPc are indicative for stronger recombination losses in this material system. This can be ascribed to a significantly lower hole mobility in neat CuPc as compared to DIP[31,60] and to a further reduction of the mobility in C_{60}:CuPc blends due to the small scale phase separation (see Ref.[45]) By contrast, the morphology of the DIP phase in both architectures (PHJ and PM-HJ) is characterized by large, cohesive crystalline structures, allowing for favorable transport properties and thus less recombination losses.[61]

6. Conclusions

In conclusion, we have presented a comprehensive analysis of the new donor material diindenoperylene (DIP) in combination with the fullerene C_{60} ranging from growth studies and energy level alignment via electrical transport properties and finally to its successful application in organic solar cells. Our studies emphasize the crucial influence of the substrate temperature during DIP film growth on the morphology and thus the overall performance of DIP based photovoltaic cells. Growth at elevated temperature leads to the formation of a cohesive network of crystalline DIP domains, yielding a large surface area that can be covered with C_{60} molecules in planar heterojunctions, or to a phase separated bicontinuous network in bulk heterojunctions when DIP and C_{60} are coevaporated. Favorable film morphology together with high crystalline order allows for improved transport properties of both excitons and charges in photovoltaic cells. The main advantage of DIP can be found in its high ionization potential and the favorable energy level alignment with both the PEDOT:PSS electrode and the C_{60} acceptor leading to high open circuit voltages of up to 0.93 V under 100 mW cm^{-2} simulated AM1.5G illumination. Simply stacked PHJ devices – devoid of doped transport layers – yield remarkably high fill factors up to 74% and a power conversion efficiency close to 4%.

For future work, it will be important to improve the absorption properties of films incorporating DIP as donor material while keeping its good transport properties and favorable energy level alignment with C_{60}. One promising strategy might be found in modifying the orientation of the molecules: Achieving flat lying DIP molecules (so-called λ-phase[40]) could yield an increase in the absorption coefficient by a factor of ≈ 6[62,63] holding a large potential for further increasing solar cell efficiencies. Furthermore, the combination with a second donor-acceptor system absorbing in the longer wavelength range in a tandem cell could boost power conversion efficiencies to application relevant values.[64–67]

7. Experimental Section

Photovoltaic cells were fabricated on commercially available photolithographically structured tin-doped indium oxide (ITO)-coated glass substrates (Merck, sheet resistance per square <10 Ω) which were subsequently cleaned in ultra sonic bath with acetone and isopropanol prior to processing. An oxygen plasma treatment was implemented to improve wetability for the aqueous suspension of the intrinsically conducting polymer poly(3,4-ethylenedioxythiophene):poly(styrenesulfonate) (PEDOT:PSS in a ratio of 1:6 by weight, purchased from H. C. Starck as Clevios P AI4083). The polymer was deposited via spin coating, and annealed at 125 °C for 45 min under ambient conditions.

DIP (purchased from W. Schmidt Institut für PAH-Forschung) and C_{60} (purchased from Creaphys) have been twice purified by vacuum gradient sublimation prior to use, while BCP (purchased from Acros Organics) was used as-received. Materials were sequentially grown by vacuum thermal evaporation at base pressures of 10^{-6}–10^{-7} mbar with the following rates: DIP (0.5 Ås^{-1} in neat film, 0.3 Ås^{-1} in blend), C_{60} (0.5 Ås^{-1} in neat film, 0.3 Ås^{-1} in blend), BCP (0.2 Ås^{-1}), LiF (0.2 Ås^{-1}), and Al (1 Ås^{-1}). The metal cathodes (typically 1000 Å thick) were evaporated through a shadow mask resulting in solar cells with an area of 4 mm^2. The entire cell preparation as well as the electrical measurements has been performed without air exposure; i.e., under inert gas atmosphere or in vacuum.

Current-voltage characteristics were recorded using a source measure unit (Keithley 236 SMU) in dark and under illumination with a solar simulator (Oriel 150W with AM 1.5G filters). The illumination intensity was approved by a calibrated silicon reference cell (RERA systems, PV Measurement Facility, Radboud University Nijmegen, area 1 × 1 cm^2). Nevertheless, as the perfect homogeneity of the light beam cannot be guaranteed, the power conversion efficiency of our OPVCs with an area smaller than the reference cell might be slightly overestimated. Furthermore, the measured photocurrents have not been corrected for spectral mismatch.

Absorption spectra were obtained from transmission measurements of organic films grown on transparent substrates using a Varian Cary 50 UV-Vis spectrophotometer with a spectral range from 280 to 1000 nm. AFM measurements were performed using a Thermo Microscopes Autoprobe CP-Research in non-contact mode. X-ray reflectivity measurements were conducted on a GE/Seifert X-ray diffractometer (Cu K$_1$ radiation, multilayer mirror, and double bounce compressor monochromator). Grazing incidence X-ray diffraction measurements were performed on the X04SA beamline at the Swiss Light Source, Paul Scherrer Institut, Villigen, Switzerland (12 keV photon energy). X-ray scattering, AFM, and optical absorption measurements were performed under ambient conditions on solar cell relevant substrates.

Ultraviolet photoelectron spectroscopy (UPS) measurements were performed at the endstation SurICat at the synchrotron radiation source BESSY II–HZB. Spectra were recorded with a hemispherical energy analyzer (resolution set to 100 meV) with 35 eV photon energy. The secondary electron cut-off (SECO) was recorded with the sample biased at −10 V to clear the analyzer work function. By repeated measurements performed with the samples kept in dark and with additional visible light illumination we established that sample charging did not occur. Two different hole injection layers were used in the UPS experiments: Clevios P AI4083 (designated as PEDOT:PSS) and Clevios HIL1.3 (designated as HIL1.3) as a PEDOT-containing dispersion for HILs provided by H. C. Starck.[68] Both hole injection layers were deposited on cleaned ITO via spin coating, and annealed at 200 °C for 5 minutes under ambient conditions. Samples were introduced subsequently into UHV conditions where deposition of C_{60} and DIP followed (substrates at room temperature), from resistively heated crucibles with evaporation rates of ca. 1 Å min^{-1}. The film thickness was monitored with a quartz crystal microbalance. Sample transfer between preparation chamber (base pressure <3 × 10^{-8} mbar) and analysis chamber (base pressure 1 × 10^{-10} mbar) was done without breaking UHV conditions.

Supporting Information

Supporting Information is available from the Wiley Online Library or from the author.

Acknowledgements

[1] A. K. Ghosh, T. Feng, *J. Appl. Phys.* **1973**, *44*, 2781.

[2] C. W. Tang, *Appl. Phys. Lett.* **1986**, *48*, 183.

[3] J. J. M. Halls, C. A. Walsh, N. C. Greenham, E. A. Marseglia, R. H. Friend, S. C. Moratti, A. B. Holmes, *Nature* **1995**, *376*, 498.

[4] G. Yu, J. Gao, J. C. Hummelen, F. Wudl, A. J. Heeger, *Science* **1995**, *270*, 1789.

[5] M. A. Green, K. Emery, Y. Hishikawa, W. Warta, *Prog. Photovolt: Res. Appl.* **2010**, *18*, 346.

[6] http://www.solarmer.com (accessed May 2010).

[7] http://www.heliatek.com. (accessed May 2010).

[8] B. P. Rand, J. G. Xue, S. Uchida, S. R. Forrest, *J. Appl. Phys.* **2005**, *98*, 124902.

[9] A. Opitz, M. Bronner, W. Brütting, *J. Appl. Phys.* **2007**, *101*, 063709.

[10] M. M. Mandoc, W. Veurman, L. J. A. Koster, B. Boer, P. W. M. Blom, *Adv. Funct. Mater.* **2007**, *17*, 2167.

[11] M. Schubert, C. Yin, M. Castellani, S. Bange, T. L. Tam, A. Sellinger, H.-H. Hörhold, T. Kietzke, D. Neher, *J. Chem. Phys.* **2009**, *130*, 094703.

[12] B. P. Rand, J. Genoe, P. Heremans, J. Poortmans, *Prog. Photovolt: Res. Appl.* **2007**, *15*, 659.

[13] P. Peumans, S. Uchida, S. R. Forrest, *Nature* **2003**, *425*, 158.

[14] S. Yoo, B. Domercq, B. Kippelen, *Appl. Phys. Lett.* **2004**, *85*, 5427.

[15] K. Schulze, C. Uhrich, R. Schüppel, K. Leo, M. Pfeiffer, P. Bäuerle, E. Brier, E. Reinold, *Adv. Mater.* **2006**, *18*, 2872.

[16] A. Opitz, J. Wagner, M. Bronner, W. Brütting, A. Hinderhofer, F. Schreiber, *Phys. Status Solidi A* **2009**, *206*, 2683.

[17] K. Vandewal, K. Tvingstedt, A. Gadisa, O. Inganäs, J. V. Manca, *Nat. Mater.* **2009**, *8*, 904.

[18] P. A. van Hal, R. A. J. Janssen, G. Lanzani, G. Cerullo, M. Zavelani-Rossi, S. D. Silvestri, *Chem. Phys. Lett.* **2001**, *345*, 33.

[19] P. Peumans, S. R. Forrest, *Appl. Phys. Lett.* **2001**, *79*, 126.

[20] S. M. Schultes, P. Sullivan, S. Heutz, B. M. Sanderson, T. S. Jones, *Mat. Sci. Eng. C–Biomim.* **2005**, *25*, 858.

[21] W. J. Potscavage, S. Yoo, B. Kippelen, *Appl. Phys. Lett.* **2008**, *93*, 193308.

[22] M. F. Lo, T. W. Ng, T. Z. Liu, V. A. L. Roy, S. L. Lai, M. K. Fung, C. S. Lee, S. T. Lee, *Appl. Phys. Lett.* **2010**, *96*, 113303.

[23] A. Wilke, T. Mizokuro, R.-P. Blum, J. P. Rabe, N. Koch, *IEEE J. Sel. Top. Quant.* **2010**, in press.

[24] A. K. Tripathi, J. Pflaum, *Appl. Phys. Lett.* **2006**, *89*, 082103.

[25] D. Kurrle, J. Pflaum, *Appl. Phys. Lett.* **2008**, *92*, 133306.

[26] S. B. Rim, P. Peumans, *J. Appl. Phys.* **2008**, *103*, 124515.

[27] R. R. Lunt, N. C. Giebink, A. A. Belak, J. B. Benziger, S. R. Forrest, *J. Appl. Phys.* **2009**, *105*, 053711.

[28] S. Banerjee, A. P. Parhi, S. S. K. Iyer, S. Kumar, *Appl. Phys. Lett.* **2009**, *94*, 223303.

[29] A. C. Dürr, F. Schreiber, M. Münch, N. Karl, B. Krause, V. Kruppa, H. Dosch, *Appl. Phys. Lett.* **2002**, *81*, 2276.

[30] R. R. Lunt, J. B. Benziger, S. R. Forrest, *Adv. Mater.* **2010**, *22*, 1233.

[31] N. Karl, *Synth. Met.* **2003**, *133–134*, 649.

[32] D. Fujishima, H. Kanno, T. Kinoshita, E. Maruyama, M. Tanaka, M. Shirakawa, K. Shibata, *Sol. Energy Mater. Sol. Cell.* **2009**, *93*, 1029.

[33] R. Schueppel, K. Schmidt, C. Uhrich, K. Schulze, D. Wynands, J. L. Bredas, E. Brier, E. Reinold, H. B. Bu, P. Bäuerle, B. Männig, M. Pfeiffer, K. Leo, *Phys. Rev. B* **2008**, *77*, 085311.

[34] D. Wynands, B. Männig, M. Riede, K. Leo, E. Brier, E. Reinold, P. Bäuerle, *J. Appl. Phys.* **2009**, *106*, 054509.

[35] C. M. Ramsdale, J. A. Barker, A. C. Arias, J. D. MacKenzie, R. H. Friend, N. C. Greenham, *J. Appl. Phys.* **2002**, *92*, 4266.

[36] M. Svensson, F. Zhang, S. C. Veenstra, W. J. H. Verhees, J. C. Hummelen, J. M. Kroon, O. Inganäs, and M. R. Andersson, *Adv. Mater.* **2003**, *15*, 988.

[37] T. Kietzke, D. A. M. Egbe, H.-H. Hörhold, D. Neher, *Macromolecules* **2006**, *39*, 4018.

[38] Z. E. Ooi, T. L. Tam, R. Y. C. Shin, Z.-K. Chen, T. Kietzke, A. Sellinger, M. Baumgarten, K. Muellen, J. C. deMello, *J. Mater. Chem.* **2008**, *18*, 4619.

[39] R. A. Marsh, C. Groves, N. C. Greenham, *J. Appl. Phys.* **2007**, *101*, 083509.

[40] A. C. Dürr, N. Koch, M. Kelsch, A. Rühm, J. Ghijsen, R. L. Johnson, J.-J. Pireaux, J. Schwartz, F. Schreiber, H. Dosch, A. Kahn, *Phys. Rev. B* **2003**, *68*, 115428.

[41] A. C. Dürr, F. Schreiber, K. A. Ritley, V. Kruppa, J. Krug, H. Dosch, B. Struth, *Phys. Rev. Lett.* **2003**, *90*, 016104.

[42] N. Koch, *ChemPhysChem* **2007**, *8*, 1438.

[43] N. Koch, A. Vollmer, A. Elschner, *Appl. Phys. Lett.* **2007**, *90*, 043512.

[44] R. W. Lof, M. A. Vanveenendaal, B. Koopmans, H. T. Jonkman, G. A. Sawatzky, *Phys. Rev. Lett.* **1992**, *68*, 3924.

[45] A. Opitz, J. Wagner, W. Brütting, I. Salzmann, N. Koch, J. Manara, J. Pflaum, A. Hinderhofer, F. Schreiber, *IEEE J. Sel. Top. Quant.* **2010**, in press.

[46] B. P. Rand, D. P. Burk, and S. R. Forrest, *Phys. Rev. B* **2007**, *75*, 115327.

[47] S. M. Sze, *Physics of Semiconductor Devices*, 3rd ed., Wiley, New York, **1981**.

[48] C. Uhrich, D. Wynands, S. Olthof, M. K. Riede, K. Leo, S. Sonntag, B. Maennig, M. Pfeiffer, *J. Appl. Phys.* **2008**, *104*, 043107.

[49] J. Nelson, J. Kirkpatrick, P. Ravirajan, *Phys. Rev. B* **2004**, *69*, 035337.

[50] A. Kumar, S. Sista, Y. Yang, *J. Appl. Phys.* **2009**, *105*, 094512.

[51] P. Peumans, V. Bulović, S. R. Forrest, *Appl. Phys. Lett.* **2000**, *76*, 2650.

[52] N. Li, B. E. Lassiter, R. R. Lunt, G. Wei, S. R. Forrest, *Appl. Phys. Lett.* **2009**, *94*, 023307.

[53] H. Gommans, B. Verreet, B. P. Rand, R. Muller, J. Poortmans, P. Heremans, J. Genoe, *Adv. Funct. Mater.* **2008**, *18*, 3686.

[54] J. G. Xue, B. P. Rand, S. Uchida, S. R. Forrest, *Adv. Mater.* **2005**, *17*, 66.

[55] J. G. Xue, B. P. Rand, S. Uchida, S. R. Forrest, *J. Appl. Phys.* **2005**, *98*, 124903.

[56] T. Kirchartz, K. Taretto, U. Rau, *J. Phys. Chem. C* **2009**, *113*, 17958.

[57] P. Sullivan, S. Heutz, S. M. Schultes, T. S. Jones, *Appl. Phys. Lett.* **2004**, *84*, 1210.

[58] S. Heutz, P. Sullivan, B. M. Sanderson, S. M. Schultes, T. S. Jones, *Sol. Ener. Mater. Sol. Cell.* **2004**, *83*, 229.

[59] P. Peumans, S. R. Forrest, *Appl. Phys. Lett.* **2001**, *79*, 126.

[60] R. W. I. de Boer, A. F. Stassen, M. F. Craciun, C. L. Mulder, A. Molinari, S. Rogge, A. F. Morpurgo, *Appl. Phys. Lett.* **2005**, *86*, 262109.

[61] C. Deibel, *Phys. Status Solidi A* **2009**, *206*, 2731.

[62] U. Heinemeyer, R. Scholz, L. Gisslén, M. I. Alonso, J. O. Ossó, M. Garriga, A. Hinderhofer, M. Kytka, S. Kowarik, A. Gerlach, F. Schreiber, *Phys. Rev. B* **2008**, *78*, 085210.

[63] L. Gisslen, R. Scholz, *Phys. Rev. B* **2009**, *80*, 115309

[64] J. Y. Kim, K. Lee, N. E. Coates, D. Moses, T. Q. Nguyen, M. Dante, A. J. Heeger, *Science* **2007**, *317*, 222.

[65] T. Ameri, G. Dennler, C. Lungenschmied, C. J. Brabec, *Energy Environ. Sci.* **2009**, *2*, 347.

[66] P. Peumans, A. Yakimov, S. R. Forrest, *J. Appl. Phys.* **2003**, *93*, 3693.

[67] R. Timmreck, J. Meiss, A. Merten, R. Schueppel, M. Furno, C. Uhrich, W.-M. Gnehr, M. Pfeiffer, M. Riede, K. Leo, *Proc. EU PVSEC 24*, **2009**, 89.

[68] Product datasheet available at http://www.clevios.com (accessed May 2010).